

histopathology; Y.S., K.N., T.T. and M.T. performed the SNP array analysis; T.A. and H.K. generated *NDRG2*-deficient mice; M.H. and K.N. performed the cDNA microarray analysis; K.N. and Y.K. performed the DNA methylation array analysis; K.S. provided patient samples; I.K. Y.A., T.T., A.H., and H.S. edited and commented on the manuscripts; S.N. and K.M. wrote the manuscript; K.M. supervised the project.

Additional information

Accession codes: The gene expression data have been deposited in the Gene Expression Omnibus database under accession code GSE43017.

Supplementary Information accompanies this paper at <http://www.nature.com/naturecommunications>

Competing financial interests: The authors declare no competing financial interests.

Reprints and permission information is available online at <http://npg.nature.com/reprintsandpermissions/>

How to cite this article: Nakahata, S. *et al.* Loss of *NDRG2* expression activates PI3K-AKT signalling via PTEN phosphorylation in ATLL and other cancers. *Nat. Commun.* 5:3393 doi: 10.1038/ncomms4393 (2014).

Somatic *RHOA* mutation in angioimmunoblastic T cell lymphoma

Mamiko Sakata-Yanagimoto^{1,22}, Terukazu Enami^{1,22}, Kenichi Yoshida^{2,3,22}, Yuichi Shiraishi⁴, Ryohei Ishii⁵, Yasuyuki Miyake¹, Hideharu Muto¹, Naoko Tsuyama⁶, Aiko Sato-Otsubo^{2,3}, Yusuke Okuno², Seiji Sakata⁷, Yuhei Kamada¹, Rie Nakamoto-Matsubara¹, Nguyen Bich Tran¹, Koji Izutsu^{8,9}, Yusuke Sato^{2,3}, Yasunori Ohta¹⁰, Junichi Furuta¹¹, Seiichi Shimizu¹², Takuya Komeno¹³, Yuji Sato¹⁴, Takayoshi Ito¹⁵, Masayuki Noguchi¹⁶, Emiko Noguchi¹⁷, Masashi Sanada^{2,3}, Kenichi Chiba⁴, Hiroko Tanaka¹⁸, Kazumi Suzukawa^{1,19}, Toru Namoku¹⁹, Yuichi Hasegawa¹, Osamu Nureki⁵, Satoru Miyano^{4,18}, Naoya Nakamura²⁰, Kengo Takeuchi^{6,7}, Seishi Ogawa^{2,3,23} & Shigeru Chiba^{1,21,23}

Angioimmunoblastic T cell lymphoma (AITL) is a distinct subtype of peripheral T cell lymphoma characterized by generalized lymphadenopathy and frequent autoimmune-like manifestations^{1,2}. Although frequent mutations in *TET2*, *IDH2* and *DNMT3A*, which are common to various hematologic malignancies^{3,4}, have been identified in AITL^{5–8}, the molecular pathogenesis specific to this lymphoma subtype is unknown. Here we report somatic *RHOA* mutations encoding a p.Gly17Val alteration in 68% of AITL samples. Remarkably, all cases with the mutation encoding p.Gly17Val also had *TET2* mutations. The *RHOA* mutation encoding p.Gly17Val was specifically identified in tumor cells, whereas *TET2* mutations were found in both tumor cells and non-tumor hematopoietic cells. *RHOA* encodes a small GTPase that regulates diverse biological processes. We demonstrated that the Gly17Val *RHOA* mutant did not bind GTP and also inhibited wild-type *RHOA* function. Our findings suggest that impaired *RHOA* function in cooperation with preceding loss of *TET2* function contributes to AITL-specific pathogenesis.

AITL accounts for approximately 20% of all T cell lymphoma cases¹. On the basis of gene expression profiling, the normal counterparts of AITL tumor cells are proposed to be follicular helper T cells (T_{FH} cells), a subset of helper T cells^{1,2}. Peripheral T cell lymphoma,

not otherwise specified (PTCL-NOS) represents a more heterogeneous category of mature T cell lymphomas, including a subset sharing some features of AITL^{5,9}.

To explore the relevant gene mutations responsible for the pathogenesis of AITL, we performed whole-exome sequencing¹⁰ of three AITL and three PTCL-NOS samples (Supplementary Table 1). Of the targeted sequence, 86.5% was analyzed by ≥ 20 independent reads on average (Supplementary Figs. 1 and 2). In total, we identified and confirmed 87 non-silent somatic mutations (4–27 (median of 12.5) per sample) by Sanger sequencing and/or deep sequencing (Fig. 1a and Supplementary Table 2), including 79 missense and 5 nonsense single-nucleotide variants (SNVs) and 1 non-frameshift and 2 frameshift deletions. The numbers of non-silent mutations were lower than reported in B cell neoplasms^{11,12}, although relatively low tumor contents, which were suspected owing to mutant allele frequencies of generally less than 0.25 (median of 0.11), could have compromised sensitivity in detecting mutations (Fig. 1a). Recurrent mutations were found in only one gene, *RHOA*, in which identical c.50G>T mutations predicted to result in a p.Gly17Val alteration were identified in one PTCL-NOS and three AITL specimens (Fig. 1a,b and Supplementary Fig. 3). No allelic imbalances were observed at the *RHOA* locus (Supplementary Fig. 4).

Prompted by this discovery, we screened *RHOA* mutations in an extended cohort of 72 AITL and 87 PTCL-NOS samples by

¹Department of Hematology, Faculty of Medicine, University of Tsukuba, Tsukuba, Japan. ²Cancer Genomics Project, Graduate School of Medicine, The University of Tokyo, Tokyo, Japan. ³Department of Pathology and Tumor Biology, Graduate School of Medicine, Kyoto University, Kyoto, Japan. ⁴Laboratory of DNA Information Analysis, Human Genome Center, Institute of Medical Science, The University of Tokyo, Tokyo, Japan. ⁵Department of Biophysics and Biochemistry, Graduate School of Science, The University of Tokyo, Tokyo, Japan. ⁶Division of Pathology, Cancer Institute, Japanese Foundation for Cancer Research, Tokyo, Japan. ⁷Pathology Project for Molecular Targets, Cancer Institute, Japanese Foundation for Cancer Research, Tokyo, Japan. ⁸Department of Hematology, Toranomon Hospital, Tokyo, Japan. ⁹Okinaka Memorial Institute for Medical Research, Tokyo, Japan. ¹⁰Department of Pathology, Toranomon Hospital, Tokyo, Japan. ¹¹Department of Dermatology, Faculty of Medicine, University of Tsukuba, Tsukuba, Japan. ¹²Department of Hematology, Tsuchiura Kyodo General Hospital, Tsuchiura, Japan. ¹³Department of Hematology, Mito Medical Center, National Hospital Organization, Mito, Japan. ¹⁴Department of Hematology, Tsukuba Memorial Hospital, Tsukuba, Japan. ¹⁵Department of Hematology, JA Toride Medical Center, Toride, Japan. ¹⁶Department of Pathology, Faculty of Medicine, University of Tsukuba, Tsukuba, Japan. ¹⁷Department of Medical Genetics, Faculty of Medicine, University of Tsukuba, Tsukuba, Japan. ¹⁸Laboratory of Sequence Analysis, Human Genome Center, Institute of Medical Science, The University of Tokyo, Tokyo, Japan. ¹⁹Department of Clinical Laboratory, University of Tsukuba Hospital, Tsukuba, Japan. ²⁰Department of Pathology, Tokai University School of Medicine, Isehara, Japan. ²¹Life Science Center, Tsukuba Advanced Research Alliance, University of Tsukuba, Tsukuba, Japan. ²²These authors contributed equally to this work. ²³These authors jointly directed this work. Correspondence should be addressed to S.C. (schiba-t@md.tsukuba.ac.jp) or S.O. (sogawa-ky@umin.ac.jp).

Received 13 May 2013; accepted 12 December 2013; published online 12 January 2014; doi:10.1038/ng.2872



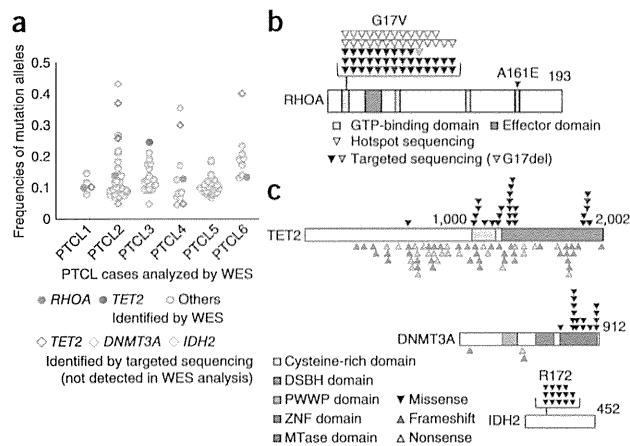


Figure 1 Discovery of a *RHOA* mutation encoding p.Gly17Val in PTCL by whole-exome sequencing. (a) Somatic mutations identified in three AITL and three PTCL-NOS samples are shown with the frequencies of mutation alleles plotted. Red and blue filled circles indicate the *RHOA* mutation encoding p.Gly17Val and *TET2* mutations, respectively. Mutations of *TET2*, *IDH2* and *DNMT3A* that were not found by whole-exome sequencing (WES) but were identified later by targeted deep sequencing are also depicted by open diamonds: blue, *TET2*; orange, *DNMT3A*; purple, *IDH2*. (b) Positions of *RHOA* alterations. Nucleotide-binding domains are represented by yellow boxes. The effector domain is represented by a red box. (c) Positions of alterations in the *TET2*, *DNMT3A* and *IDH2* proteins. Black, red and yellow arrowheads indicate missense, frameshift and nonsense mutations, respectively. The cysteine-rich and double-strand β -helix (DSBH) domains of *TET2* are represented by a yellow and a red box, respectively. proline-tryptophan-tryptophan-proline (PWWP), zinc-finger (ZNF) and methyltransferase (MTase) domains of *DNMT3A* are shown by light blue, blue and purple boxes, respectively.

deep sequencing of all coding sequences ($n = 79$) or the mutational hotspot (c.50G>T; p.Gly17Val) ($n = 80$) of *RHOA* (Supplementary Fig. 1 and Supplementary Table 3). *RHOA* mutations were found in 66 of the 159 specimens, with a much higher frequency in AITL (51/72; 70.8%) than PTCL-NOS (15/87; 17.2%) (Fig. 1b, Table 1 and Supplementary Table 4). We identified no *RHOA* mutations other than the c.50G>T (p.Gly17Val) mutation except for an in-frame deletion (c.49_51delGGA) resulting in a p.Gly17del (PTCL33) alteration and a missense SNV (c.482C>A) resulting in a p.Ala161Glu (PTCL59) alteration in cases negative for the p.Gly17Val alteration (Fig. 1b and Supplementary Table 4). We validated all low-frequency mutant *RHOA* alleles (frequency of 0.02–0.05) using an independent deep sequencing platform (Online Methods). No *RHOA* mutations encoding p.Gly17Val were found in other hematologic malignancies, including in myeloid neoplasms ($n = 142$), mature B cell neoplasms ($n = 91$) and mature T cell neoplasms other than AITL and PTCL-NOS ($n = 11$) (Table 1), suggesting that the *RHOA* mutation encoding p.Gly17Val is highly specific to AITL and PTCL-NOS among hematologic malignancies.

According to the pathologic definition in the Online Methods^{5,9}, we classified 21 of 59 immunohistochemically characterized PTCL-NOS cases as T_{FH} -like PTCL-NOS cases. Thirteen of the 21 T_{FH} -like PTCL-NOS cases (61.9%) had the *RHOA* mutation encoding p.Gly17Val, whereas none of the remaining 38 PTCL-NOS cases had this mutation ($P < 0.001$) (Supplementary Table 5). Given that almost all AITL cases showed T_{FH} -like features, these findings implied a strong correlation between the *RHOA* mutation encoding p.Gly17Val and the T_{FH} -like phenotype of PTCL, similar to the correlation previously shown between *TET2* mutations and the T_{FH} -like phenotype of PTCL⁵. No clinical parameters were significantly different in

the mutation-positive and mutation-negative cases (Supplementary Fig. 5 and Supplementary Table 6).

To investigate the correlation between mutations in *RHOA* and other genes, we also resequenced *TET2*, *IDH1*, *IDH2* and *DNMT3A* in addition to *RHOA* in the subcohort of 79 PTCL (AITL, 46; PTCL-NOS, 33) cases (Supplementary Figs. 1 and 6). A total of 97 *TET2* mutations were identified in 54 of the 79 PTCL specimens (68.4%) (AITL, 38 (82.6%); PTCL-NOS, 16 (48.5%)). Similarly, we found *DNMT3A* mutations in 21 PTCL specimens (26.6%) (AITL, 12 (26.0%); PTCL-NOS, 9 (27.3%)). We identified *IDH2* mutations affecting Arg172 (p.Arg172Met, p.Arg172Thr, p.Arg172Ser, p.Arg172Lys and p.Arg172Gly) in 14 cases (17.7%) (AITL, 14 (30.4%); PTCL-NOS, 0 (0%)) (Figs. 1c and 2a, Supplementary Tables 7 and 8, and Supplementary Note). No *IDH1* mutations were identified. Several mutations in *TET2*, *IDH2* and *DNMT3A*, which had escaped detection in the whole-exome sequencing analysis, were newly identified in the same whole-exome sequencing cohort by this targeted resequencing. Our inability to detect these mutations using whole-exome sequencing might be explained by their low allelic mutational burdens and/or by low sequencing coverage in whole-exome sequencing (Fig. 1a). Unexpectedly, however, *TET2* and *DNMT3A* mutations with high-frequency alleles were also newly found in three and two cases, respectively (Fig. 1a). The cause of our inability to identify *TET2* and *DNMT3A* mutations by whole-exome sequencing might be the presence of substantial numbers of mutant reads in the reference bone marrow samples (Supplementary Fig. 7, Supplementary Tables 9 and 10, and Supplementary Note).

Remarkably, mutations in *RHOA*, *TET2* and *IDH2* showed strong correlations; all *RHOA*-mutated cases also had *TET2* mutations ($P < 0.001$), and all but one of the *IDH2* mutations were confined to tumors also having *RHOA* and *TET2* mutations ($P < 0.001$) (Fig. 2a and Supplementary Note). The predominant *TET2* alleles showed significantly higher allelic burden than mutant *RHOA* and *IDH2* alleles in most cases (*TET2* versus *RHOA*, $P < 0.001$; *TET2* versus *IDH2*, $P = 0.001$; Fig. 2b,c), whereas *RHOA* and *IDH2* mutations had similar allele frequencies (Fig. 2d). Skewed distributions of relative allele frequencies among these mutations strongly suggested that *TET2* mutations predated *RHOA* and/or *IDH2* mutations in most cases.

Table 1 *RHOA* mutation encoding p.Gly17Val in various hematologic malignancies

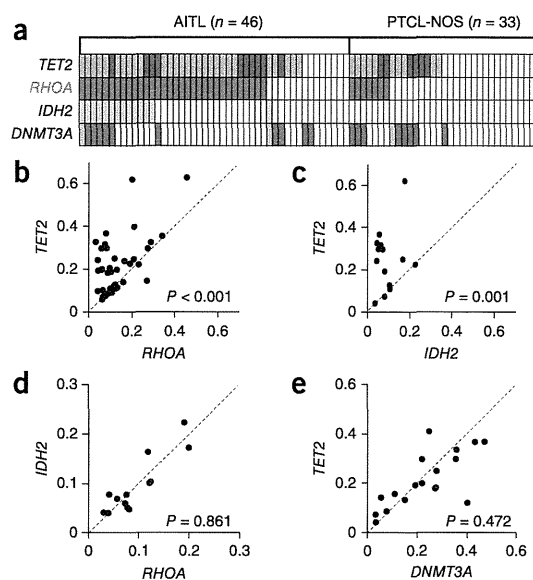
Disease	Number of mutated cases (%)
T cell malignancies	$n = 170$
AITL ^a	51/72 (70.8)
PTCL-NOS	15/87 (17.2)
with AITL features	13/21 (61.9)
without AITL features	0/38 (0)
ND ^b	2/28 (7.1)
Other T cell malignancies	0/11 (0)
B cell malignancies	$n = 91$
DLBCL	0/44 (0)
Follicular lymphoma	0/19 (0)
Other B cell malignancies	0/28 (0)
Myeloid malignancies	$n = 142$
AML	0/89 (0)
MDS	0/36 (0)
MPN	0/14 (0)
MDS/MPN	0/3 (0)

DLBCL, diffuse large B cell lymphoma; AML, acute myeloid leukemia; MDS, myelodysplastic syndrome; MPN, myeloproliferative neoplasm.

^aIncluding one case with *RHOA* p.Gly17del and one case with *RHOA* p.Ala161Glu.

^bNot determined.

Figure 2 Relationship between *RHOA*, *TET2*, *IDH2* and *DNMT3A* mutations in PTCL. (a) Distribution of mutations in *RHOA*, *TET2*, *IDH2* and *DNMT3A* in 79 PTCL (46 AITL and 33 PTCL-NOS) samples that were analyzed by targeted deep sequencing. Two or three distinct *TET2* mutations and two distinct *DNMT3A* mutations were identified in multiple samples. Dark blue and dark green indicate samples having a single *TET2* or *DNMT3A* mutation, respectively, and light blue and light green indicate samples having multiple *TET2* or *DNMT3A* mutations. (b–e) Comparison of the allele frequencies of two selected mutations in samples harboring mutations in *TET2* and *RHOA* (b), *TET2* and *IDH2* (c), *RHOA* and *IDH2* (d) and *TET2* and *DNMT3A* (e). Each axis shows the frequencies of the mutant alleles. When multiple mutations existed in a single gene, the frequencies of major alleles are indicated. Data were analyzed statistically by Wilcoxon rank-sum test.



Mutations in *DNMT3A* largely overlapped and had similar allelic burdens as *TET2* mutations (Fig. 2e), but their correlation with *RHOA* or *IDH2* mutations was much less clear (Fig. 2a).

To determine the clonal structure of the *RHOA* mutation encoding p.Gly17Val and of other gene mutations, we isolated CD4⁺ T cells, a fraction enriched for tumor cells and other fractions, from the specimens of two cases (PTCL159 and PTCL160; Supplementary Figs. 8 and 9), and we analyzed mutations by targeted resequencing as well as by Sanger sequencing. In PTCL159 (PTCL-NOS in the skin), we found the *RHOA* mutation encoding p.Gly17Val, two *TET2* mutations and a *DNMT3A* mutation (Supplementary Fig. 8 and Supplementary Table 7). Somatic origin of these mutations was confirmed (Supplementary Fig. 8). We identified the *RHOA* mutation encoding p.Gly17Val in purified CD4⁺ cells but not in CD8⁺ cells. One of the two *TET2* mutations and the *DNMT3A* mutation were identified in both CD4⁺ and CD8⁺ cell fractions with apparently similar allelic burdens to each other in the two types of cells, whereas the remaining *TET2* mutation was found only in CD4⁺ cells and was absent in CD8⁺ cells (Supplementary Fig. 8). These observations suggested that the *RHOA* mutation encoding p.Gly17Val and one of the two *TET2* mutations were confined to CD4⁺ tumor cells, whereas the other *TET2* mutation and the *DNMT3A* mutation were shared by both CD4⁺ tumor cells and CD4⁺ and CD8⁺ reactive cells (Supplementary Fig. 8). In contrast, the *RHOA* mutation encoding p.Gly17Val and two *TET2* mutations identified in PTCL160 (AITL) were all confined to tumor cells (Supplementary Fig. 9, Supplementary Table 7 and Supplementary Note). These data indicate that the *RHOA* mutation encoding p.Gly17Val was a specific event in tumor cells. In contrast,

TET2 and *DNMT3A* mutations seemed to have taken place in either CD4⁺ tumor cells or early progenitor cells such as those that give rise to all hematopoietic cells, as previously described^{6,7}.

RHOA encodes a small GTPase, which has a highly conserved amino acid structure across species (Supplementary Fig. 10). *RHOA* operates as a molecular switch that regulates a wide variety of biological processes through cycling between an active (GTP-bound) state and an inactive (GDP-bound) state^{13,14}. *RHOA* is activated by specific guanine-exchange factors (GEFs) that catalyze the dissociation of GDP and the rebinding of GTP, and signaling is terminated by hydrolysis of GTP to GDP, a reaction that is stimulated by GTPase-activating proteins (GAPs)^{13,14}.

Three-dimensional model structures of the Gly17Val *RHOA* protein suggest compromised binding to GDP and GTP^{15,16} (Supplementary Fig. 11 and Supplementary Note). In fact, when we expressed *RHOA* proteins in NIH3T3 cells, a substantial fraction of wild-type *RHOA* protein bound GTP or GTPγS in a rhotekin pulldown assay¹⁷, whereas no GTP- or GTPγS-bound form was pulled down for the Gly17Val *RHOA* mutant (Fig. 3a), suggesting severely reduced GTP and GTPγS binding by the Gly17Val mutant.

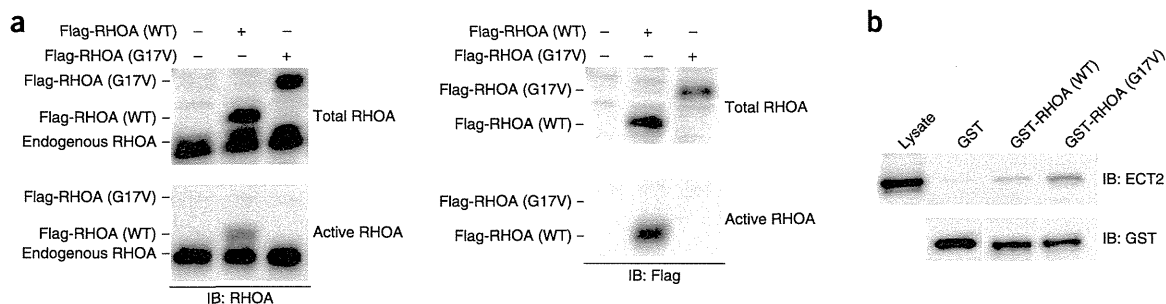


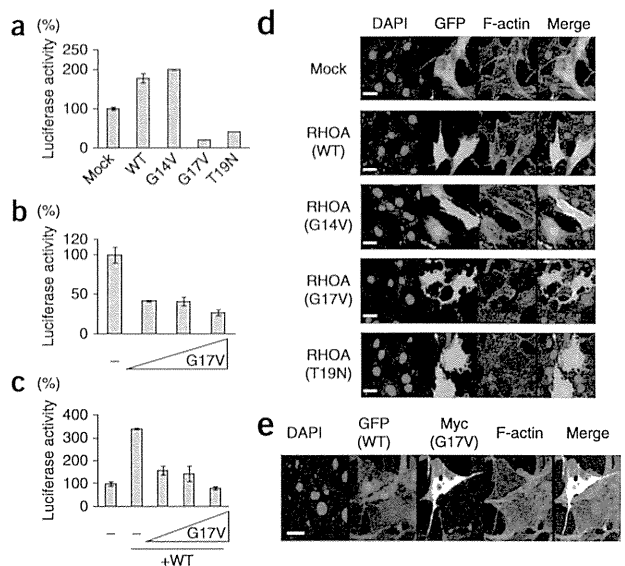
Figure 3 Dominant-negative effect of the Gly17Val *RHOA* mutant on wild-type *RHOA*. (a) Rhotekin pulldown assay for endogenous *RHOA* and exogenously expressed wild-type and Gly17Val *RHOA* in NIH3T3 cells. Extracts from NIH3T3 cells expressing Flag-tagged wild-type or Gly17Val *RHOA* were pulsed with GTPγS and incubated with glutathione Sepharose beads on which the RHO-binding domain of rhotekin fused to GST was immobilized, and precipitated protein was blotted with antibodies to *RHOA* (left) and Flag (right) to detect active *RHOA* specifically. IB, immunoblot; WT, wild type. (b) GEF-binding activity of wild-type and Gly17Val *RHOA*. Lysate from NIH3T3 cells, transiently expressing ECT2 with an N-terminal deletion, was incubated with Sepharose beads on which GST-fused wild-type or Gly17Val *RHOA* protein was immobilized, and precipitated protein was blotted with antibody to ECT2.

LETTERS

Figure 4 Effects of the Gly17Val RHOA mutant on transcriptional regulation and actin cytoskeleton formation in NIH3T3 cells. (a–c) Effect of Gly17Val RHOA on the transcriptional activity of the SRF-RE. (a) Activity of the SRF-RE reporter in NIH3T3 cells expressing wild-type or mutant (Gly14Val, Gly17Val or Thr19Asn) RHOA protein. (b) Effect of increasing amounts (16, 48 or 144 ng/well) of Gly17Val RHOA on SRF-RE reporter activity in NIH3T3 cells. (c) Effect of increasing amounts (16, 48 or 144 ng/well) of Gly17Val RHOA on SRF-RE reporter activity enhanced by exogenously expressed wild-type RHOA. In each plot in a–c, the mean \pm s.d. of triplicate experiments is shown. A representative result from three independent experiments is shown. (d,e) Effect of Gly17Val RHOA on actin cytoskeleton formation. (d) F-actin staining with phalloidin (red) in NIH3T3 cells transiently transfected with vector expressing wild-type or mutant (Gly14Val, Gly17Val or Thr19Asn) RHOA. GFP is used as a marker for transduction with each cDNA. (e) NIH3T3 cells stably expressing wild-type RHOA were transfected with vector expressing Myc-tagged Gly17Val RHOA. Scale bars in d,e, 30 μ m.

Moreover, the Gly17Val RHOA mutant reduced GTP binding by both the endogenous and exogenous wild-type RHOA proteins in a dose-dependent manner (Supplementary Figs. 12 and 13), suggesting a dominant-negative nature for Gly17Val RHOA. This view was further supported by the finding that the Gly17Val RHOA mutant bound ECT2, one of the RhoGEFs, more tightly than wild-type RHOA, as was previously described for Gly17Ala RHOA¹⁸ (Fig. 3b and Supplementary Note). The Gly17del and Ala161Glu mutants also showed impaired binding capacity for GTP/GTP γ S and inhibited GTP binding by wild-type RHOA protein (Supplementary Fig. 14). Together, these results support the notion that the RHOA mutants contribute to the pathogenesis of PTCL through the inhibition of wild-type RHOA in a dominant-negative manner, although the amount of mutant RHOA protein seemed to be low in both NIH3T3 cells and primary AITL tumor cells (Supplementary Fig. 15, Supplementary Table 11 and Supplementary Note), for an unknown reason.

In accordance with these findings, unlike wild-type RHOA and mutant Gly14Val RHOA, the Gly17Val RHOA mutant did not activate transcription from the serum response factor-responsive element (SRF-RE)¹⁹ (Fig. 4a,b) and instead repressed transcription from SRF-RE activated by exogenously expressed wild-type RHOA (Fig. 4c), as did a known dominant-negative mutant of RHOA (Thr19Asn) (Fig. 4a and data not shown). Gly17Val as well as Thr19Asn RHOA also attenuated actin stress fiber formation in NIH3T3 cells, which was markedly induced by wild-type and Gly14Val RHOA²⁰ (Fig. 4d). Furthermore, the Gly17Val RHOA mutant inhibited the assembly of actin stress fibers in NIH3T3 cells



stably expressing wild-type RHOA (Fig. 4e). All these data suggest that the Gly17Val mutant functions in a dominant-negative manner with respect to wild-type RHOA.

To investigate the effect of wild-type and Gly17Val RHOA on T cells, we established Jurkat cells inducibly expressing wild-type or Gly17Val RHOA (Fig. 5a). When wild-type RHOA was expressed, the proliferation of Jurkat cells was significantly decreased (WT Dox (+) versus Mock DOX (+), $P < 0.001$, days 2–4; Fig. 5b), and G1-to-S cell cycle progression was suppressed (Supplementary Fig. 16). In contrast, inducibly expressed Gly17Val RHOA did not affect the growth or cell cycle progression of Jurkat cells (Fig. 5b and Supplementary Fig. 16). We further performed mRNA sequencing analysis to examine the effect of the RHOA mutation encoding p.Gly17Val on gene expression, using RNA prepared from Jurkat cells inducibly expressing wild-type or Gly17Val RHOA or mock-transfected cells, as well as RNA from NIH3T3 cells transiently expressing wild-type or Gly17Val RHOA or mock-transfected cells. Gene Set Enrichment Analysis (GSEA)^{21,22} demonstrated that the serum response factor (SRF) pathway, known to be activated under RHOA signaling²³, was significantly enriched at a false discovery rate (FDR) q value less than 0.25 for cells expressing wild-type RHOA versus mock-transfected cells in both Jurkat and NIH3T3 cells

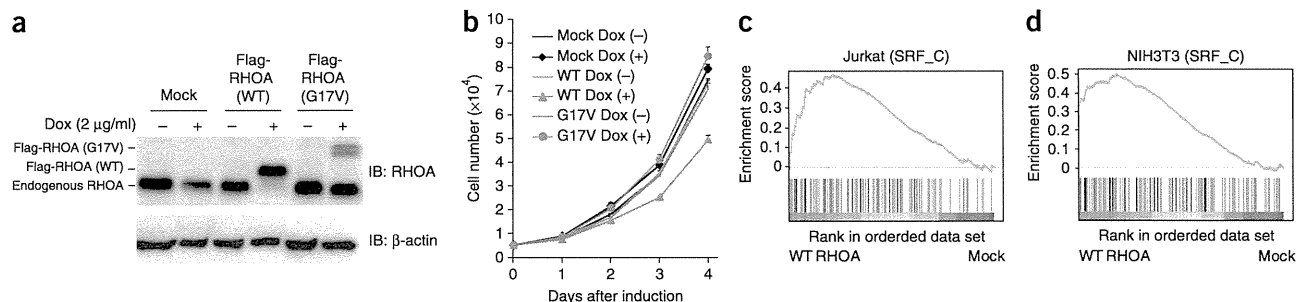


Figure 5 Effect of Gly17Val RHOA on T cells. (a) Doxycycline (Dox)-induced expression of wild-type and Gly17Val RHOA in Jurkat cells. A protein blot with antibody to RHOA is shown. β -actin is used as a loading control. (b) Proliferation of Jurkat cells inducibly expressing wild-type or Gly17Val RHOA. Absorbance (at 450 nm) was converted to cell number. The mean \pm s.d. of quadruplicate experiments is shown. A representative result from three independent experiments is shown. (c,d) GSEA for Jurkat cells inducibly expressing wild-type or Gly17Val RHOA or mock transfected and NIH3T3 cells transiently expressing wild-type or Gly17Val RHOA or mock transfected ($n = 2$ each). The SRF pathway was differentially enriched in both Jurkat cells (c) and NIH3T3 cells (d). SRF_C refers to the V\$SRF_C gene set.

(Fig. 5c,d and Supplementary Table 12). The SRF pathway was reported as an essential mediator of T cell development in the thymus^{24,25}, although we found no clue to its functional relevance in AITL development in the literature. We did not observe enrichment of the SRF pathway in either cell type expressing Gly17Val RHOA compared to mock-transfected cells or cells expressing wild-type RHOA. These findings further support the notion that Gly17Val RHOA is a loss-of-function mutant.

The extremely high frequency and specificity of the *RHOA* mutation encoding p.Gly17Val in AITL and AITL-related PTCL cases unequivocally underscore its major role in the development of these subtypes of PTCL (Supplementary Fig. 17). The finding of somatic mutation of *RHOA* in lymphoma, particularly of a mutation with a loss-of-function and/or dominant-negative nature, was rather unexpected because the oncogenic potential of *RHOA* has been implicated in human cancers²⁶. However, several lines of evidence previously suggested a tumor-suppressive role for *RHOA* in T-lineage cells^{26,27}. Moreover, transgenic expression of C3 transferase, an inhibitor of the Rho family of proteins (*RHOA*, *RHOB* and *RHOC*) under the *Lck* promoter has been shown to induce thymic T cell lymphoma in mice²⁸. Our observations in Jurkat cells expressing wild-type *RHOA* are also along these lines. Clearly, further studies are warranted to clarify the molecular pathogenesis mediated by the unique *RHOA* mutation encoding p.Gly17Val in AITL and related PTCL, and such studies might have promising implications for the development of novel diagnostics and therapeutics.

URLs. European Genome-phenome Archive, <https://www.ebi.ac.uk/ega/>; Genomon-exome, <http://genomon.hgc.jp/exome/en/index.html>; Picard, <http://picard.sourceforge.net/>; dbSNP131, <http://www.ncbi.nlm.nih.gov/projects/SNP/>; 1000 Genomes Project, <http://www.1000genomes.org/>; MSigDB, <http://www.broadinstitute.org/gsea/msigdb>.

METHODS

Methods and any associated references are available in the online version of the paper.

Accession codes. Genome sequence data are available at the European Genome-phenome Archive under accession EGAS00001000557.

Note: Any Supplementary Information and Source Data files are available in the online version of the paper

ACKNOWLEDGMENTS

We thank Y. Okoshi, N. Obara, Y. Yokoyama, H. Nishikii, N. Kurita and M. Seki for contributing to sample collection and banking. We also thank Y. Sakashita and T. Takahashi for technical assistance, and S. Narumiya and I. Kitabayashi for efficient discussion. This work was supported by Grants-in-Aid for Scientific Research (KAKENHI) from the Ministry of Education, Culture, Sports, Science and Technology of Japan (22134006 to S.O.; 22130002, 24390241, 25112703 and 25670444 to S.C.; 25461407 to M.S.-Y.) and was supported by the Sagawa Foundation for Promotion of Cancer Research, the Naito Foundation, the Mochida Memorial Foundation for Medical and Pharmaceutical Research (M.S.-Y.).

AUTHOR CONTRIBUTIONS

M.S.-Y. prepared DNA samples, sorted the tumor cells, resequenced the samples, and sorted and integrated information. T.E. analyzed the function of wild-type and mutant *RHOA*. K.Y. resequenced the samples and contributed to the resequencing data analyses. Y. Shiraiishi, E.N., K.C., H.T. and S.M. performed bioinformatics analyses of the resequencing data. R.I. and O.N. created the model structure for mutant *RHOA*. Y.M., H.M., Y.K., R.N.-M., N.B.T., K.S., T.N., Y.H. and M.N. contributed to sample collection and preparation. N.T., S. Sakata, N.N. and K.T. immunostained specimens and performed pathohistological analyses. Y. Okuno and M.S. contributed to the resequencing. A.S.-O. and Yusuke Sato

contributed to mRNA sequencing. K.I., Y. Ohta, J.F., S. Shimizu, T.K., Yuji Sato and T.I. collected samples. M.S.-Y., T.E., K.Y., S.O. and S.C. generated figures and tables, and wrote the manuscript. All authors participated in discussions and interpretation of the data and results.

COMPETING FINANCIAL INTERESTS

The authors declare no competing financial interests.

Reprints and permissions information is available online at <http://www.nature.com/reprints/index.html>.

1. Swerdlow, S.H. *et al.* *WHO Classification of Tumors of Haematopoietic and Lymphoid Tissues* 4th edn, 306–311 (IARC Press, Lyon, France, 2008).
2. de Leval, L. *et al.* The gene expression profile of nodal peripheral T-cell lymphoma demonstrates a molecular link between angioimmunoblastic T-cell lymphoma (AITL) and follicular helper T (TFH) cells. *Blood* **109**, 4952–4963 (2007).
3. Delhommeau, F. *et al.* Mutation in *TET2* in myeloid cancers. *N. Engl. J. Med.* **360**, 2289–2301 (2009).
4. Mardis, E.R. *et al.* Recurring mutations found by sequencing an acute myeloid leukemia genome. *N. Engl. J. Med.* **361**, 1058–1066 (2009).
5. Lemonnier, F. *et al.* Recurrent *TET2* mutations in peripheral T-cell lymphomas correlate with TFH-like features and adverse clinical parameters. *Blood* **120**, 1466–1469 (2012).
6. Quivoron, C. *et al.* *TET2* inactivation results in pleiotropic hematopoietic abnormalities in mouse and is a recurrent event during human lymphomagenesis. *Cancer Cell* **20**, 25–38 (2011).
7. Couronné, L., Bastard, C. & Bernard, O.A. *TET2* and *DNMT3A* mutations in human T-cell lymphoma. *N. Engl. J. Med.* **366**, 95–96 (2012).
8. Cairns, R.A. *et al.* *IDH2* mutations are frequent in angioimmunoblastic T-cell lymphoma. *Blood* **119**, 1901–1903 (2012).
9. Bustelo, X.R., Sauzeau, V. & Berenjeno, I.M. GTP-binding proteins of the Rho/Rac family: regulation, effectors and functions *in vivo*. *Bioessays* **29**, 356–370 (2007).
10. Yoshida, K. *et al.* Frequent pathway mutations of splicing machinery in myelodysplasia. *Nature* **478**, 64–69 (2011).
11. Chapman, M.A. *et al.* Initial genome sequencing and analysis of multiple myeloma. *Nature* **471**, 467–472 (2011).
12. Morin, R.D. *et al.* Frequent mutation of histone-modifying genes in non-Hodgkin lymphoma. *Nature* **476**, 298–303 (2011).
13. Bustelo, X.R., Sauzeau, V. & Berenjeno, I.M. GTP-binding proteins of the Rho/Rac family: regulation, effectors and functions *in vivo*. *Bioessays* **29**, 356–370 (2007).
14. Etienne-Manneville, S. & Hall, A. Rho GTPases in cell biology. *Nature* **420**, 629–635 (2002).
15. Ihara, K. *et al.* Crystal structure of human RhoA in a dominantly active form complexed with a GTP analogue. *J. Biol. Chem.* **273**, 9656–9666 (1998).
16. Shimizu, T. *et al.* An open conformation of switch I revealed by the crystal structure of a Mg²⁺-free form of RHOA complexed with GDP. Implications for the GDP/GTP exchange mechanism. *J. Biol. Chem.* **275**, 18311–18317 (2000).
17. Reid, T. *et al.* Rhotekin, a new putative target for Rho bearing homology to a serine/threonine kinase, PKN, and rhophilin in the rho-binding domain. *J. Biol. Chem.* **271**, 13556–13560 (1996).
18. Arthur, W.T., Ellerbroek, S.M., Der, C.J., Burridge, K. & Wennerberg, K. XPLN, a guanine nucleotide exchange factor for RhoA and RhoB, but not RhoC. *J. Biol. Chem.* **277**, 42964–42972 (2002).
19. Cheng, Z. *et al.* Luciferase reporter assay system for deciphering GPCR pathways. *Curr. Chem. Genomics* **4**, 84–91 (2010).
20. Ridley, A.J. & Hall, A. The small GTP-binding protein rho regulates the assembly of focal adhesions and actin stress fibers in response to growth factors. *Cell* **70**, 389–399 (1992).
21. Subramanian, A. *et al.* Gene set enrichment analysis: a knowledge-based approach for interpreting genome-wide expression profiles. *Proc. Natl. Acad. Sci. USA* **102**, 15545–15550 (2005).
22. Mootha, V.K. *et al.* PGC-1 α -responsive genes involved in oxidative phosphorylation are coordinately downregulated in human diabetes. *Nat. Genet.* **34**, 267–273 (2003).
23. Hill, C.S., Wynne, J. & Treisman, R. The Rho family GTPases RhoA, Rac1, and CDC42Hs regulate transcriptional activation by SRF. *Cell* **81**, 1159–1170 (1995).
24. Mylona, A. *et al.* The essential function for serum response factor in T-cell development reflects its specific coupling to extracellular signal-regulated kinase signaling. *Mol. Cell. Biol.* **31**, 267–276 (2011).
25. Fleige, A. *et al.* Serum response factor contributes selectively to lymphocyte development. *J. Biol. Chem.* **282**, 24320–24328 (2007).
26. Karlsson, R., Pedersen, E.D., Wang, Z. & Brakebusch, C. Rho GTPase function in tumorigenesis. *Biochim. Biophys. Acta* **1796**, 91–98 (2009).
27. Hébert, M. *et al.* Rho-ROCK-dependent ezrin-radixin-moesin phosphorylation regulates Fas-mediated apoptosis in Jurkat cells. *J. Immunol.* **181**, 5963–5973 (2008).
28. Cleverley, S.C., Costello, P.S., Henning, S.W. & Cantrell, D.A. Loss of Rho function in the thymus is accompanied by the development of thymic lymphoma. *Oncogene* **19**, 13–20 (2000).



ONLINE METHODS

Subjects and samples. Samples were obtained from individuals with AITL or PTCL-NOS, as well as from individuals with other mature T cell, mature B cell and myeloid neoplasms, and were used after approval was obtained from the local ethics committees at all participating institutes (**Supplementary Tables 1 and 3**). Informed consent was obtained from all living subjects. High-molecular-weight genomic DNA was extracted from archived specimens that were frozen fresh or after fixation. DNA was also extracted from paraffin-embedded, formalin-fixed samples for targeted amplicon sequencing. Constitutional DNA samples were obtained from buccal swabs, mononuclear cells from apparently tumor-free bone marrow aspirates or peripheral blood. Data on clinical outcomes were available for 71 subjects. Samples of a subcohort of PTCL-NOS cases were reviewed by four expert hematopathologists.

Within PTCL-NOS cases, a subgroup without the typical morphology of AITL but having two or more of the following immunostaining features was designated T_{FH}-like PTCL-NOS^{5,9}: (i) positive staining for CD10 in tumor cells, (ii) positive staining for PD-1 in tumor cells, (iii) proliferation of CD21-positive follicular dendritic cells and (iv) the presence of EBER-positive B cells.

Sorting of the tumor cell-enriched fraction and other fractions. CD4⁺ and CD8⁺ T cell fractions were purified from skin tumors from subject PTCL159, and CD4⁺ and CD8⁺ T cell, CD19⁺ B cell and CD14⁺ monocyte cell fractions were purified from pleural effusion cells from subject PTCL160.

The skin tumor from subject PTCL159 was processed into single-cell suspension. Cells were stained with fluorescein isothiocyanate (FITC)-conjugated anti-CD4 antibody (BD Biosciences, 555346) and phycoerythrin (PE)-conjugated anti-CD8 antibody (Dako, clone DK25) and were then fractionated on a FACSARIA (BD Biosciences).

Mononuclear cells (MNCs) were isolated from the pleural effusion of subject PTCL160 by Ficoll-Paque density-gradient centrifugation. MNCs were stained with FITC-conjugated anti-CD4 antibody and anti-CD14 antibody (BD Biosciences, 555397), PE-conjugated anti-CD8 antibody and PE-conjugated anti-CD19 antibody (Dako, clone HD37) and were fractionated on a FACSARIA.

Whole-exome sequencing. Tumor DNA was extracted from subject biopsy samples infiltrated with lymphoma cells. DNA from either buccal mucosa, bone marrow MNCs without apparent lymphoma infiltration or peripheral blood cells was used for the paired normal control. Whole-exome capture was accomplished through the hybridization of sonicated genomic DNA to the bait cDNA library synthesized on magnetic beads (SureSelect Human All Exon 50Mb or V4 kit, Agilent Technologies). Captured targets were subjected to massively parallel sequencing using a HiSeq 2000 (Illumina) according to the standard protocol for 100-bp paired-end reads.

Detection of candidate somatic mutations was performed using our in-house pipeline for whole-exome sequencing¹⁰ with minor modifications. Briefly, sequencing reads were first aligned to the human reference genome (hg19) using Burrows-Wheeler Aligner (BWA)²⁹ version 0.5.8 with default parameter settings. PCR duplicates were eliminated using Picard. The number of reads containing SNVs and indels in both tumor and germline samples was determined using SAMtools³⁰, and the null hypothesis of equal allele frequencies in tumor and germline samples was tested using the two-tailed Fisher's exact test. A variant was adopted as a candidate somatic mutation if it had $P < 0.01$, was observed in bidirectional reads (i.e., in both the plus and minus strands of the reference sequence) and its allele frequency was less than 0.1 in the corresponding germline sample. Finally, the list of candidate somatic mutations was generated by excluding synonymous SNVs and other variants registered in either dbSNP131, the 1000 Genomes Project or our in-house SNP database constructed from 180 individual samples. All candidates were validated by deep sequencing.

Validation of whole-exome analysis. Genomic DNA from tumors and paired normal samples was amplified using the REPLI-g mini kit (Qiagen). Regions that included candidate mutations were amplified by genomic PCR using KOD cox neo (TOYOBO) with a NotI linker attached to each primer

(**Supplementary Table 13**). Products were combined, and DNA was purified using the QIAquick PCR Purification kit (Qiagen) and digested with NotI. Digested DNA was purified again, and a 1.5- μ g aliquot of purified DNA was ligated with T4 DNA ligase for 5 h, sonicated into ~150-bp fragments on average using Covaris and used for the generation of sequencing libraries, according to a modified Illumina paired-end library protocol. Libraries were then subjected to deep sequencing on a MiSeq (Illumina) according to the standard protocol for 150-bp paired-end reads.

Data processing and variant calling were performed with a set of modifications to the method described in a previous publication¹⁰. Each read was aligned to the set of targeted sequences from PCR amplification, for which BLAT³¹, instead of BWA²⁹, was used with the -fine option. Mapping information in the .psl format was converted to the .sam format with paired-read information using an in-house-generated my_psl2sam script. The script was derived from the psl2sam.pl script distributed with SAMtools. Minor changes were applied to the original script to give the paired-end information upon conversion. Of the successfully mapped reads, the following reads were excluded from further analysis: reads that mapped to multiple sites, reads that mapped with more than four mismatched bases and reads that had more than ten soft-clipped bases. Next, the Estimation_CRME script was run to eliminate strand-specific errors and to exclude cycle-dependent errors. A strand-specific mismatch ratio was calculated for each nucleotide variant for both strands using data for those bases between 11 and 50 cycles. To calculate the frequency of each SNV, all reads were mapped to the target reference sequence using BLAT. The number of mapped reads was differentially enumerated for the dichotomic alleles, i.e., mutant and wild-type alleles. For indels, individual reads were first aligned to each of the wild-type and indel sequences and then assigned to the one with which better alignment was obtained in terms of the number of matched bases. Allele frequency was calculated by enumerating each allele according to those assignments. SNVs comprising equal to or more than 2.0% of total reads of the tumor sample rather than the germline sample at each nucleotide position, if it existed, were adopted as somatic mutations.

Targeted sequencing of the RHOA, TET2, IDH1, IDH2 and DNMT3A genes. Targeted sequencing was performed to determine the mutation rate in a large series of PTCL samples for the RHOA, TET2, IDH1, IDH2 and DNMT3A genes. DNA samples from 79 tumors (46 AITL and 33 PTCL-NOS) and 9 paired bone marrow or peripheral blood cell samples were analyzed, including 6 pairs of tumors and controls analyzed by whole-exome sequencing.

DNA samples were prepared as follows: 61 DNA samples were extracted from fresh frozen biopsy specimens, and 18 DNA samples were extracted from paraformaldehyde-lysine-periodate (PLP)-fixed frozen specimens (46 samples were original DNA, and 33 samples were amplified using the REPLI-g mini kit). All exons of the selected genes were captured with the SureSelect target enrichment system (Agilent Technologies), and massively parallel sequencing was then performed on a HiSeq 2000.

For each sample, all sequencing reads were aligned to hg19 using BWA version 0.5.8 with default parameters. After all duplicated reads and low-quality reads and bases were removed, allele frequencies of SNVs and indels were calculated at each genomic position by enumerating the relevant reads using SAMtools. Initially, all variants showing allele frequencies of >0.02 were extracted and annotated with ANNOVAR³² for further consideration if they were found in >6 reads out of >10 total reads and appeared in both plus- and minus-strand reads. All synonymous variants, known SNPs in public and private databases, including dbSNP131, the 1000 Genomes Project as of 21 May 2012 and our in-house database, were removed. Candidate mutations whose allele frequencies were <5% were validated by PCR-based deep sequencing using Ion Torrent (Life Technologies).

Deep sequencing using Ion Torrent. Fragmented DNA was prepared in the same manner as described above. Libraries were then subjected to deep sequencing on Ion Torrent according to the standard protocol for 300-bp single-end reads. After excluding reads whose length was >200 bases or <50 bases to reduce sequencing errors, the allele frequency was calculated for each SNV or indel as described above.

Hotspot sequencing to identify *RHOA* mutations encoding p.Gly17Val. Eighty DNA samples from tumors were extracted from unfixed biopsy specimens ($n = 1$), PLP-fixed frozen specimens ($n = 38$) and formalin-fixed, paraffin-embedded specimens ($n = 41$). All samples were original DNA without amplification, except for one sample amplified using the REPLI-g mini kit. Samples were subjected to genomic PCR with tagged PCR primers (Supplementary Table 14) and were subsequently prepared using the NEBNext DNA Library-Prep Reagent Set for Illumina (New England BioLabs). Products underwent massively parallel sequencing on a MiSeq according to the manufacturer's protocol. The SNV representing a G-to-T change comprising equal to or more than 2.0% of total reads at the c.G50 nucleotide position of the *RHOA* gene was adopted as the mutation. Methods of data analysis were the same as described above.

Antibodies. Antibodies used for protein blots or immunostaining were mouse anti-RhoA (1:1,000; Cytoskeleton, ARH03), mouse anti- β -actin (1:2,000; Sigma, A5441), mouse anti-DDDDK tag (1:10,000; MBL, M185-3), mouse anti-Myc tag (1:10,000 for WB, 1:500 for IHC; MBL, M192-3), mouse anti-GST tag (1:2,000; MBL, M071-3), rabbit anti-ECT2 (1:1,000; Millipore, 07-1364), goat anti-mouse IgG conjugated to horseradish peroxidase (HRP) (1:10,000; Dako, P0447), goat anti-rabbit IgG conjugated to HRP (1:10,000; Dako, P0448) and Alexa Fluor 647-conjugated goat anti-mouse IgG (1:1,000; Invitrogen, A-21235).

Cell lines and transfection. NIH3T3 cells (American Type Culture Collection) were cultured at 37 °C in low-glucose DMEM (Sigma) supplemented with 10% heat-inactivated FCS and 1% penicillin-streptomycin. Cells were transfected with plasmids using FuGene6 transfection reagent (Promega) according to the manufacturer's protocol. Jurkat cells (European Collection of Cell Cultures) were cultured at 37 °C in RPMI-1640 (Sigma) supplemented with 10% FCS and 1% penicillin-streptomycin.

Mutagenesis and constructs. Human *RHOA* cDNA was isolated by PCR amplification from peripheral blood MNC-derived cDNA. Mutagenesis to create constructs encoding the Gly14Val, Gly17Val, Gly17del, Thr19Asn and Ala161Glu mutants was carried out with the PrimeStar Mutagenesis Basal kit (TaKaRa) according to the manufacturer's instructions. All cDNA-encoded products were tagged at their N terminus with the Flag and/or c-Myc epitope. These constructs were subcloned into the pEF-neo expression vector, the pGCDN-samIRESGFP retroviral vector and the tetracycline-inducible lentivirus-based expression vector CS-TRE-PRE-Ubc-tTA-I2G7 (ref. 33). cDNA encoding the ECT2-GFP fusion protein was kindly provided by T. Ishizaki (Oita University). An N-terminal deletion mutant (residues 414–882) of ECT2 was generated with the PrimeStar Mutagenesis Basal kit. Constructs encoding wild-type and Gly17Val RHOA were subcloned into the pGEX-2tk vector (GE Healthcare). All cDNA sequences were confirmed by Sanger sequencing.

Retrovirus production and generation of stable cell lines. For retrovirus production, each retroviral vector was transfected into 293gp packaging cells with a vesicular stomatitis virus G (VSV-G) expression plasmid³⁴. Retrovirus-containing supernatant was used for the transduction of 293gp cells to establish stable cell lines capable of producing high titers of VSV-G pseudotyped retroviral particles. To establish cell lines stably expressing wild-type or mutant RHOA, NIH3T3 cells were infected with these retroviruses. Infected cells expressing GFP were isolated using a FACSAria. The purity of sorted cell fractions consistently exceeded 95%.

Rhotekin binding assays. The amount of the GTP-bound form of the RHOA protein was measured using the RhoA Activation Assay kit (Cytoskeleton) according to the manufacturer's instructions. Briefly, cell lysate was incubated at 4 °C for 1 h with a GST fusion protein containing the RHO-binding domain of rhotekin (GST-RBD) immobilized on glutathione Sepharose beads. After washing the beads twice with lysis buffer and once with wash buffer provided by the manufacturer, we fractionated bead-bound proteins by 12% SDS-PAGE and immunoblotted with anti-RHOA and anti-Flag antibodies. Total cell lysate was also blotted with anti-RHOA and anti-Flag antibodies to assess the fractional ratios of rhotekin-bound RHOA proteins.

GEF-binding assays. GST-fused wild-type and Gly17Val RHOA proteins were prepared as previously described with minor modification³⁵. Briefly, GST-fused wild-type and Gly17Val RHOA proteins were expressed in BL21 competent *Escherichia coli* cells (TaKaRa), which were lysed in lysis buffer (20 mM HEPES, pH 7.5, 150 mM NaCl, 5 mM MgCl₂, 1% Triton X-100, 1 mM dithiothreitol and 1 mM phenylmethylsulfonyl fluoride) and subjected to sonication. Lysate was cleared by centrifugation at 20,000g for 15 min at 4 °C, incubated with Glutathione Sepharose 4B beads (GE healthcare) for 45 min at 4 °C and washed twice with lysis buffer.

NIH3T3 cells were transiently transfected with a construct expressing the N-terminal deletion mutant of ECT2 by FuGene6. After 48 h, cells were lysed in lysis buffer, cleared by centrifugation and incubated with GST-fused wild-type or Gly17Val RHOA protein bound to Sepharose beads for 2 h. Beads were washed three times with lysis buffer. Bound material was boiled with Laemmli buffer and blotted with anti-GST and anti-ECT2 antibodies.

SRF-RE reporter assays. For the measurement of activity on SRF-RE, luciferase reporter assays were performed using the pGL4.34 reporter vector (Promega), which contains an SRF-RE and a mutant form of the serum response element lacking the ternary complex factor (TCF)-binding domain. SRF-RE was designed to respond to SRF-dependent and TCF-independent signaling such as the signaling that occurs after RhoA activation¹⁹. NIH3T3 cells were seeded in 24-well plates and cotransfected with pGL4.34 at 40 ng/well, the expression vector pSR α containing β -galactosidase at 20 ng/well and the expression vector pEF-neo containing various *RHOA* cDNA constructs at the concentrations indicated. Luciferase activity was measured at 48 h after transfection, and values were normalized by β -galactosidase activity.

F-actin staining. NIH3T3 cells were transfected with constructs encoding wild-type or mutant RHOA on glass coverslips. After 48 h, cells were fixed with 4% paraformaldehyde in PBS for 15 min at room temperature and permeabilized with 0.5% Triton X-100 in PBS for 10 min. After washing with PBS, cells were incubated with rhodamine phalloidin (100 nM; Cytoskeleton). For double-staining immunohistochemistry, permeabilized cells were blocked with 3% BSA and 0.1% Triton X-100 in PBS. Then, cells were incubated with mouse anti-Myc antibody (1:500 dilution) followed by Alexa Fluor 647-conjugated goat anti-mouse IgG antibody (1:1,000 dilution) and rhodamine phalloidin (100 nM). Nuclei were stained with DAPI. Images were obtained by confocal laser scanning microscopy (Leica).

Lentivirus production and generation of stable cell lines. For lentivirus production, each lentiviral vector was transfected into HEK293T cells with the psPAX2 packaging plasmid and the pMD2.G envelope plasmid. To establish cell lines inducibly expressing wild-type or Gly17Val RHOA, Jurkat cells were infected with these lentiviruses. Infected cells expressing GFP were sorted on a FACSAria. The purity of sorted cell fractions consistently exceeded 95%.

Cell proliferation assays. For cell growth assays, Jurkat cells transduced with lentiviral vectors were incubated in 96-well culture plates, and the absorbance at 450 nm was measured with Cell Counting Kit-8 (Dojindo) according to the manufacturer's instructions.

Cell cycle analysis. Cell cycle distributions were determined by 5-bromo-2'-deoxyuridine (BrdU) and aminoactinomycin D (AAD) incorporation using the APC BrdU Flow kit according to the manufacturer's protocol (BD Pharmingen). Briefly, Jurkat cells were incubated for 30 min in BrdU (10 μ M). Then, cells were fixed, permeabilized, treated with DNase and stained with APC-conjugated anti-BrdU antibody and 7-AAD. Flow cytometry was performed on a FACSCalibur cytometer (BD Biosciences), and data were analyzed with FlowJo software (Tree Star).

mRNA sequencing for Jurkat and NIH3T3 cells. Jurkat cells, inducibly expressing wild-type or Gly17Val RHOA, were described above. Wild-type or Gly17Val RHOA protein expression was induced by the addition of 2 μ g/ml doxycycline for 2 d ($n = 2$ for each). NIH3T3 cells were transiently transfected with pGCDNsamIRESGFP vector encoding wild-type or Gly17Val RHOA ($n = 2$ for each). After 48 h, GFP-positive cells were sorted by FACSAria.



Total RNA was extracted by RNeasy mini kit (Qiagen) using the RNase-free DNase kit (Qiagen) to reduce contamination from genomic DNA according to the manufacturer's protocol. Libraries for sequencing were prepared using the Illumina TruSeq RNA Sample Preparation kit v2, according to the manufacturer's instructions. Briefly, poly(A)⁺ RNA was recovered from 1 µg of total RNA using oligo(dT)-coated Sera-Mag magnetic beads. Recovered poly(A)⁺ RNA was then chemically fragmented. RNA fragments were converted to cDNA using SuperScript II and random primers. The second strand was synthesized using RNase H and DNA polymerase I. cDNA ends were repaired using T4 DNA polymerase, T4 polynucleotide kinase and Klenow DNA polymerase. A single adenosine was added to 3' ends using Klenow fragment (3'-to-5' exo minus). Adaptors were attached to cDNA ends using T4 DNA ligase. Fragments were then amplified by ten cycles of PCR using Phusion DNA polymerase. Libraries were validated with an Agilent 2200 TapeStation (Agilent Technologies) and were applied to an Illumina flow cell using the Illumina Cluster Station. Sequencing was performed on a HiSeq 2000 with the paired-end 100-bp read option, according to the manufacturer's instructions.

Reads obtained from RNA sequencing were mapped to the reference transcript and genome using the Genomon-fusion pipeline. For the expression

level of each gene, the fragments per kilobase of exon per million mapped reads (FPKM) value was calculated from mapped reads on the gene. GSEA was carried out using GSEA version 2.0. The top ten highest gene sets of normalized enrichment score were listed on the basis of FDR *q* values (<0.25). Curated gene sets (c2.kegg.version 4.0, c3.tft.version 4.0 and c5.bp.version 4.0) used in this study were obtained from MSigDB collections.

29. Li, H. & Durbin, R. Fast and accurate short read alignment with Burrows-Wheeler transform. *Bioinformatics* **25**, 1754–1760 (2009).
30. Li, H. *et al.* The Sequence Alignment/Map format and SAMtools. *Bioinformatics* **25**, 2078–2079 (2009).
31. Kent, W.J. BLAT—the BLAST-like alignment tool. *Genome Res.* **12**, 656–664 (2002).
32. Wang, K., Li, M. & Hakonarson, H. ANNOVAR: functional annotation of genetic variants from high-throughput sequencing data. *Nucleic Acids Res.* **38**, e164 (2010).
33. Yamaguchi, T. *et al.* Development of an all-in-one inducible lentiviral vector for gene specific analysis of reprogramming. *PLoS ONE* **7**, e41007 (2012).
34. Ory, D.S., Neugeboren, B.A. & Mulligan, R.C. A stable human-derived packaging cell line for production of high titer retrovirus/vesicular stomatitis virus G pseudotypes. *Proc. Natl. Acad. Sci. USA* **93**, 11400–11406 (1996).
35. Guilluy, C., Dubash, A.D. & Garcia-Mata, R. Analysis of RhoA and Rho GEF activity in whole cells and the cell nucleus. *Nat. Protoc.* **6**, 2050–2060 (2011).

